

Short Communication

## Corrosion Resistance and Mechanical Property Enhancement of SPCC Steel Using an Induction Heat Treatment

Chien-Hung Lin<sup>1,\*</sup>, Jia-Ren Lee<sup>2</sup>, Hung-Hua Sheu<sup>3</sup>, Sung-Ying Tsai<sup>4</sup>

<sup>1</sup> Department of Physics, ROC Military Academy, Feng-Shan, Kaohsiung, Taiwan

<sup>2</sup> Department of Physics, National Kaohsiung Normal University, Kaohsiung, Taiwan

<sup>3</sup> Department of Chemical and Materials Engineering, Chung Cheng Institute of Technology, National Defense University, Taoyuan City, Taiwan

<sup>4</sup> Materials and Electro-Optics Research Division, National Chung-Shan Institute of Science and Technology, Tao-Yuan 325, Taiwan

\*E-mail: [linhungcma@gmail.com](mailto:linhungcma@gmail.com)

Received: 24 April 2017 / Accepted: 21 June 2017 / Published: 13 August 2017

---

Rapid quenching and subsequent tempering treatment are used extensively to enhance the performance of steel in the manufacture industry. The effect of an induction heat treatment on the microstructure, mechanical properties and corrosion resistance of SPCC (Steel Plate Cold-rolled Commercial) steel is discussed in this study. The surface profile of the SPCC steel was analysed using AFM (atomic force microscopy), which showed that grain growth occurred after the induction heat treatment. The corrosion behaviour was investigated using potentiodynamic measurements in the presence of a 5 wt% NaCl solution. The corrosion current density of the SPCC steel specimens with and without a quenching treatment were  $6.66 \times 10^{-5}$  and  $3.78 \times 10^{-4}$  A/cm<sup>2</sup>, respectively. It was demonstrated that the grain refinement effectively enhanced the corrosion resistance of the SPCC steel. The stress-strain diagram, upper yield point, ductility and yield elongation shifted due to the induction heat treatment. Hence, the experimental results showed that the hardness and the tensile properties of these specimens were clearly correlated to the microstructures. A comparison between the analytical and experimental results exhibits consistent agreement. The proposed methodology improves the performance of the SPCC steel and helps to promote its development in the near future.

---

**Keywords:** SPCC steel, induction heat treatment, corrosion, grain growth, yield elongation.

### 1. INTRODUCTION

Rapid energy consumption is an urgent problem faced in the past decade. Lighter structure vehicles decrease energy demand associated with transportation. SPCC steel is a commercial material with superior mechanical properties [1] but experiences corrosion in atmospheric conditions. It has

been demonstrated that the inclusion of lanthanum and cerium (La 35% + Ce 65%) enhances the corrosion resistance of SPCC [2]. The corrosion rate of the SPCC steel decreases as greater amounts of the  $\alpha$ -FeOOH phase appear. This is due to the addition of lanthanum and cerium after 480 hours of exposure in a cyclic wet-dry experiment. The mechanical properties of SPCC steel have been investigated by using cyclic fatigue testing at a maximum stress of 350 MPa, a stress ratio of  $R=0.1$ , and a frequency of  $f=10$  Hz. Crack initiation in the SPCC specimen was performed by pre-treated using a water peening method [3]. The fatigue life of SPCC steel clearly decreased due to the presence of corrosion at the crack tip.

The surface hardness is broadly enhanced by induction heat treatments with advantages including energy savings, precision control, localized heating, high efficiency and rapid processing [4-8]. The ductility and the strength of E34 steel is enhanced by cyclic quench treatments [9]. These techniques are used to characterize the corrosion resistance of E34 steel after heat treatments, including mass loss, the potentiodynamic polarization curve, and electrochemical impedance spectroscopy. The superior performance of E34 steel has been demonstrated via grain refinement in electrochemical testing. The performance of AISI 4140 steel was modified by using an induction heat treatment and demonstrated that the appearance of the martensite phase enhanced the hardness and wear resistance of the substrate [10]. The quench rate correlated to the overall performance of the low alloy steel [11]. The presence of coarse carbide influences the mechanical behaviour through the induction heat treatment parameters and it was revealed that the cooling rate is inversely proportional to grain growth and dislocation density. The mechanical and corrosive properties of 12 MnNiVR oil tank steel were investigated in presence of a simulated environment [12] showing that quench/tempering treatment resulted in superior corrosion resistance compared to a pure quench when exposed to a 3.5 wt% NaCl environment and electrochemical testing. Additionally, the specimen subjected to the quench/tempering treatment also exhibited enhanced mechanical properties during tensile testing. The sintered nanostructure of Al-Fe powder was examined after the induction heat treatment [13]. The consolidation pressure, time and temperature for sintering were 50 MPa, 6 min and 823 K, respectively. It was shown that the crystallite size exhibited a positive correlation to the milling treatment. From the Nyquist plot, the electrochemical impedance was shown to decrease for finer Al-Fe powders in a 3.5 wt% NaCl environment. The terminal result demonstrated that the grain refinement strongly correlated to the macroscopic performance of the nanocrystalline material. Discontinuous yield behaviour in high purity iron has been observed due to the grain size being modified by the air-cooling after the annealing process [14]. The yield strength is inversely proportional to the grain size according to the Hall-Petch relationship:

$$\sigma_y = \sigma_0 + kD^{-1/2}, \quad (1)$$

where  $\sigma_0$  is the stress associated with initializing dislocation motion,  $k$  is the Hall-Petch slope,  $D$  is the mean grain size and  $\sigma_y$  is the yield stress. This finding demonstrates that the heat treatment changed the yield behaviour for a metallic material. Inner lattice deformation is caused by interstitial atoms to fill into a gap in the iron lattice. The upper and lower upper yields are caused by locking-in dislocations and the barrier for dislocation mobility, respectively. The specimen exists in the plastic stage after the loading beyond the yield value. The mechanics of yield behaviour was discussed

[15], which demonstrates that the angle between the Lüders band and its tensile axis is approximately 50 degrees. The Lüders band propagated along the axis for the initial deformation until the end of the yield stage. A discontinuous yield phenomenon is observed in the stress-strain diagram. The interaction between the mobile dislocations and interstitial atoms decrease the overall strain behaviour as a yield elongation.

While many studies have been done on SPCC steel, few studies have reported on the grain size effect of it. The goal of this research is to enhance the corrosion resistance and mechanical properties of SPCC steel under atmospheric conditions. The first topic addressed is the modification of the microstructure of the SPCC steel using various induction heat treatments. Superficial materials properties were measured by AFM (atomic force microscopy), Vickers hardness (HV), tensile testing and potentiodynamic polarization curves. Further investigations are warranted after this preliminary refinement of SPCC steel as part of the material’s development.

## 2. EXPERIMENTS

The SPCC steel sheet used in this work is a commercial quality steel subjected to a cold-rolling treatment and with a chemical composition listed in Table 1.

**Table 1.** Composition of the commercial steel (SPCC) used in this work

Element	C	Si	Mn	S	P
weight%	0.12	0.5	0.5	0.025	0.035

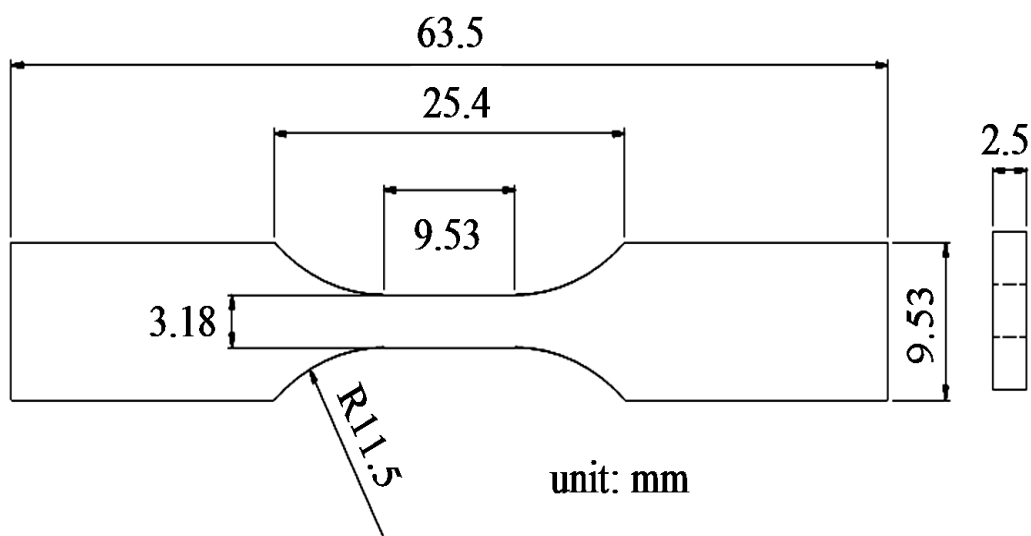


**Figure 1.** Tensile specimen geometry.

The material was machined to a 2.5 mm thick tensile specimen according to ASTM 6938 standard (as in Fig 1). This specimen exhibits an obvious yield point when tested in a uniaxial tensile

testing machine. The pretreatment included degreasing, surface cleaning and dehydration prior to the induction heat treatment. The induction heat process results vary depending on the fixed electric current, frequency and hold time. The specimen is heated by electromagnetic induction when a nearby coil is subjected to a high frequency alternative current. Eddy currents are generated on the surface of the SPCC steel due to the skin effect. The local region is joule heated due to the magnetic hysteresis loss. The induction heating parameters were maintained at 80 kHz (frequency), 10°C (heating rate), 15 kVA (power), 950°C (maximum temperature), and 2 mins (holding time). The steel is hardened by the rapid heating and cooling processes (quenching via deionised water) during the induction heat treatment. As a result, a hardened surface is obtained, and the bulk of the material retains its original material state. The tempering treatment effectively released the residual stress existing on the bulk surface during the quench crack formation and is used to improve the physical properties of hardened steel via elevated temperatures and fixed temperatures for a period of time. The tempering treatment increases the ductility and toughness of the steel via grain refinement. In this work, the temperature was increased to 300°C for 1 hour during the tempering treatment.

### *2.1 Microstructure and hardness measurements*

The morphology and the hardness of specimens were examined using atomic force microscopy (AFM) and Vickers hardness measurements. The AFM image was obtained from Park Scientific Instruments (XE-100). The tip of the cantilever was 50 nm in radius and the scan rate for the AFM testing was 1 Hz in contact mode. A commercial hardness tester DM2D (AFFRI Inc) was employed to hardness testing that a square-base diamond pyramid was pressed on the metallic surface. The loading force and holding time for the hardness measurement were 0.3 kgf and 20 seconds, respectively. All Vickers hardness results are averaged for every 5 points.

### *2.2 Potentiodynamic polarisation*

Potentiodynamic polarisation was employed to analyse the corrosion resistance of the SPCC steel using a Versastat 4 system (AMETEK Inc) using a standard three electrode cell system with an Ag/AgCl (Reference Electrode, REF), a platinum electrode (Auxiliary Electrode, AUX), and using the specimen as the working electrode. The measurement was executed in the sweeping potential mode ranging from +1 V to -1 V at a scan rate of 0.5 mV/s. The SPCC steel specimen with and without heat treatment were machined into a 1 cm<sup>2</sup> sample and exposed to a 0.5 wt% NaCl solution at ambient temperature to perform the corrosion test.

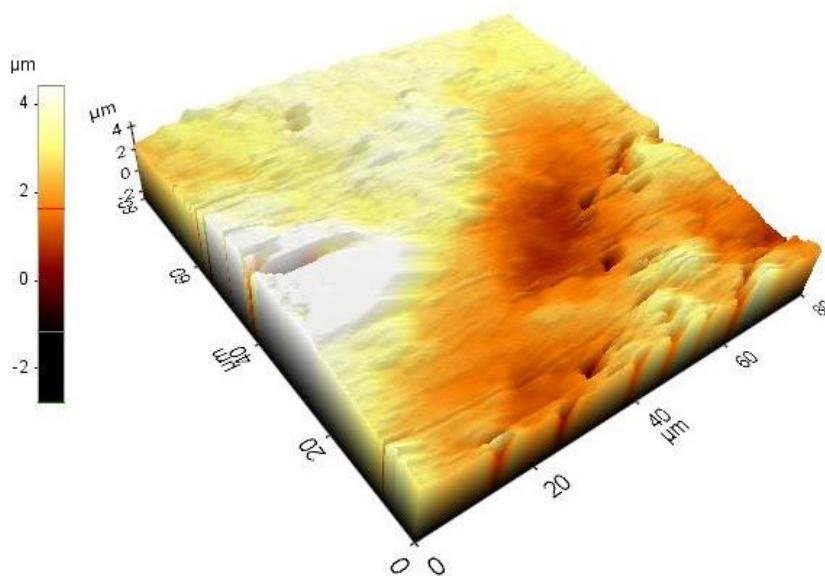
### *2.3 Tensile testing*

A servo-motor machine MTS YM-H45A2 was employed to mechanical force loading and strain behaviour characterization. The mechanical properties were characterized by tensile testing and included identification of the yield point, strain, stiffness, elastic limit and ductility. The longitudinal

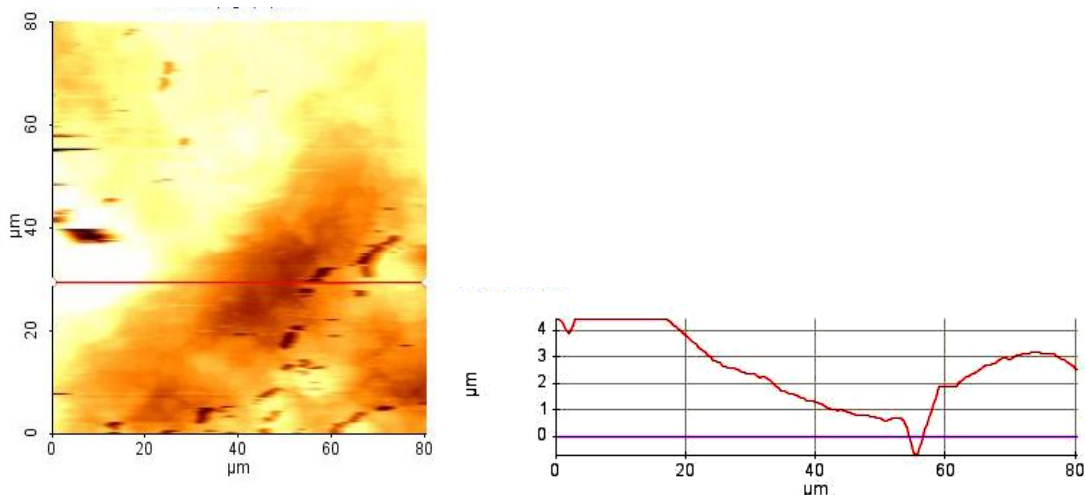
direction of test specimen was parallel to the rolling direction of the raw sheet. The specimens were loaded to a maximum stress 430 MPa at a rate of 5 mm/min.

### 3. RESULTS AND DISCUSSION

#### 3.1 Surface morphology and hardness

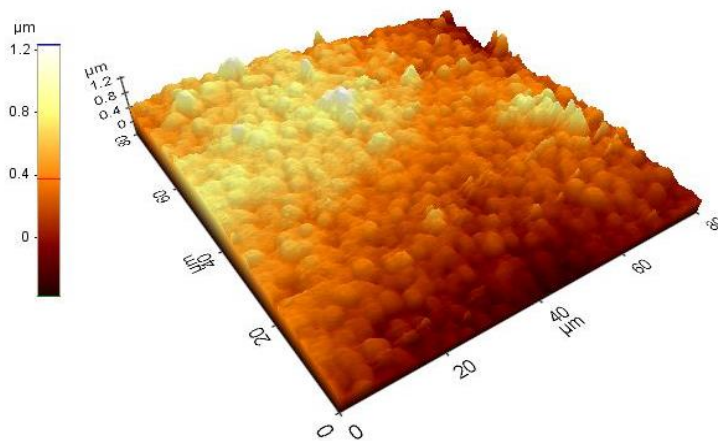


(a) Three-dimensional AFM images (80  $\mu\text{m} \times 80 \mu\text{m}$ )

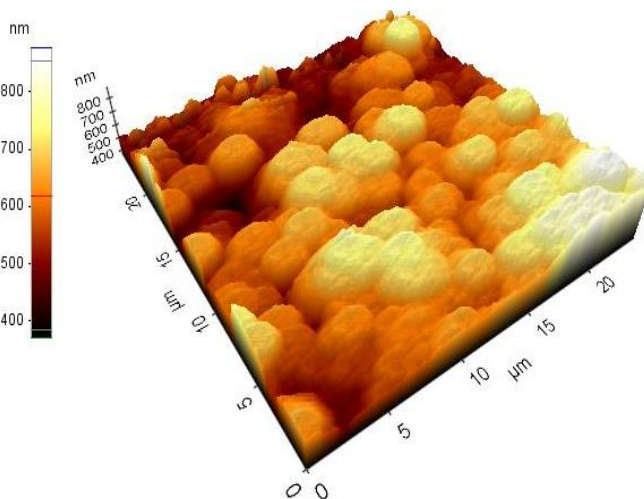


(b) Cross sectional profile along the solid line shown.

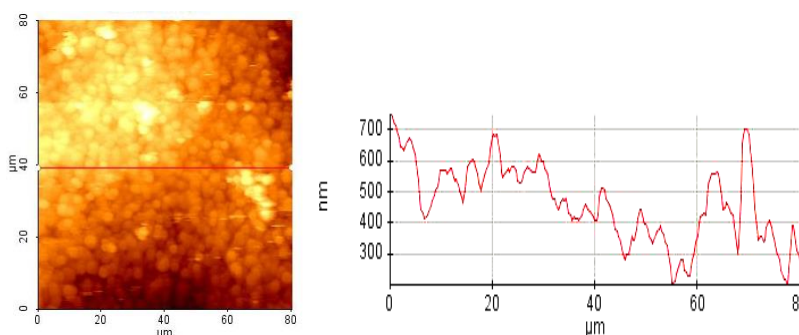
**Figure 2.** AFM micrographs showing substrate details.



(a) Three-dimensional AFM images (80  $\mu\text{m} \times 80 \mu\text{m}$ )

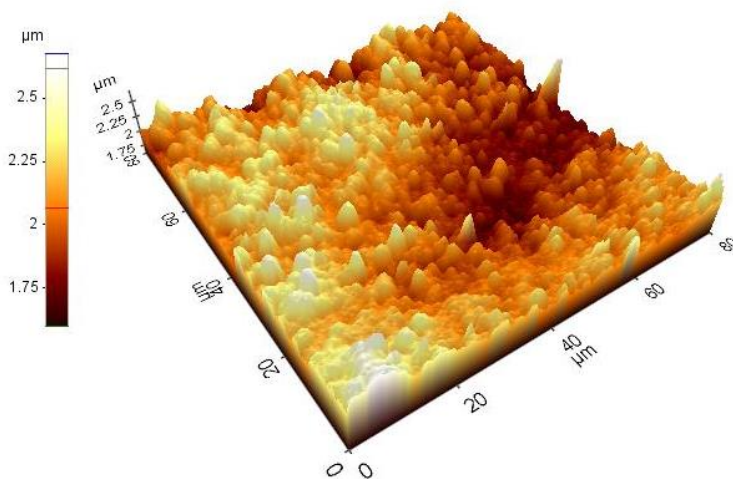


(b) Three-dimensional AFM images (24  $\mu\text{m} \times 24 \mu\text{m}$ )

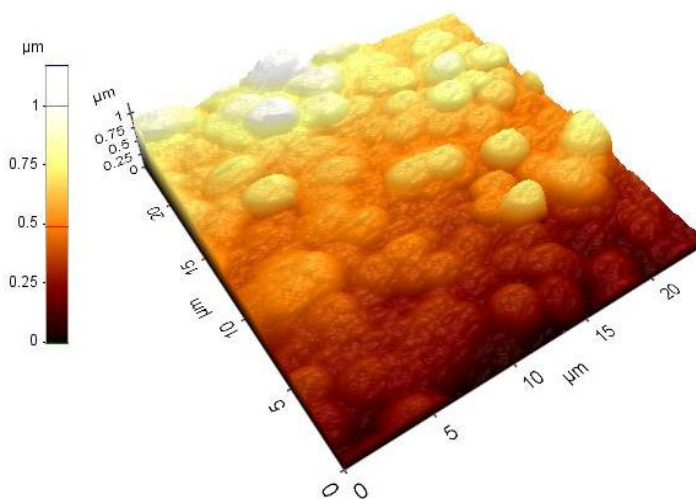


(c) Cross sectional profile along the solid line shown

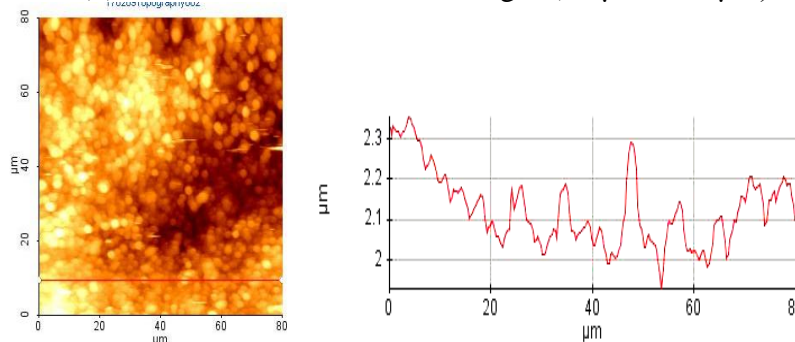
**Figure 3.** AFM micrographs showing details of the specimen subjected to the quenching treatment.



(a) Three-dimensional AFM images (80 μm × 80 μm)



(b) Three-dimensional AFM images (24 μm × 24 μm)



(c) Cross sectional profile along the solid line shown.

**Figure 4.** AFM micrographs showing details of the specimen subjected to the quenching and tempering treatment.

A surface scan of the raw material is shown in Fig 2, exhibiting a maximum profile range of approximately 5 μm in height, as shown in Fig 2(b). The SPCC steel is transformed into austenite beyond the  $A_{c3}$  line at elevated temperatures in the iron-carbon phase diagram. The carbon atom, as an

interstitial solute, exists in the lattice after rapid cooling and transforms into a saturated solid solution upon the formation of hard martensite.

**Table 2.** The Vickers hardness of the SPCC steel subjected to with various heat treatments

	Vickers Hardness (HV)					Mean
	1	2	3	4	5	
Substrate	120	138	129	132	119	127.6
Quenching	238	226	220	240	222	229.2
Quenching/Tempering	205	198	199	203	183	197.6

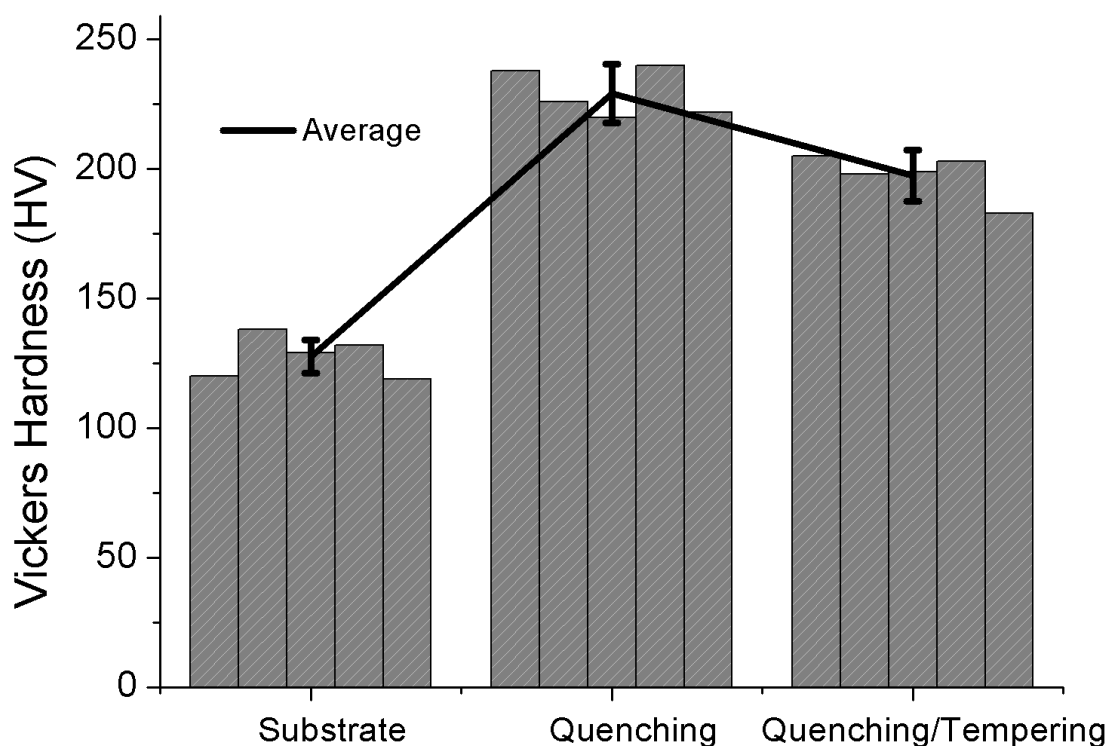


**Figure 5.** Statistical hardness measurements of the SPCC steel specimens.

The grain refinement on the SPCC steel surface after the induction heat treatment is shown in Fig 3. The maximum height range of the profile is approximately 0.5  $\mu\text{m}$ , as shown in Fig 3(b). Another specimen was treated with the tempering process after rapid cooling to modify the mechanical properties. Examples of the grain growth that occur after the subsequent tempering treatment are shown in Fig 4.

Substantial strain hardening results from the quenching process, meaning that the Vickers hardness of the SPCC steel clearly increases after the heat treatments, as shown in Fig 5. The mean Vickers hardness of the SPCC steel after quenching and the quenching/tempering processes are 229.2 HV and 197.6 HV, respectively, and as shown in Table 2.

The grain boundary effect certainly influenced the Vickers hardness of the SPCC steel and the magnitude and direction of the grains are crucial properties related to improving the hardness of the SPCC steel.

### 3.2 Corrosion resistance

Potentiodynamic polarisation was employed to analyse the corrosion resistance of the SPCC steel in an NaCl environment, with the results shown in Table 3 (corrosion potential  $E_{corr}$ , corrosion current density  $i_{corr}$ , anodic and cathodic Tafel slopes  $\beta_a$  and  $\beta_c$ ).

**Table 3.** Corrosion parameters of the SPCC steel in a 5 wt% NaCl solution

	$E_{corr}$ (V) vs SCE	$I_{corr}$ (A/cm <sup>2</sup> )	$\beta_a$ (V/dec)	$\beta_c$ (V/dec)
Substrate	-0.604	$3.78 \times 10^{-4}$	0.168	0.302
Quenching	-0.459	$6.66 \times 10^{-5}$	0.096	0.225
Quenching/Tempering	-0.467	$3.02 \times 10^{-5}$	0.144	0.271

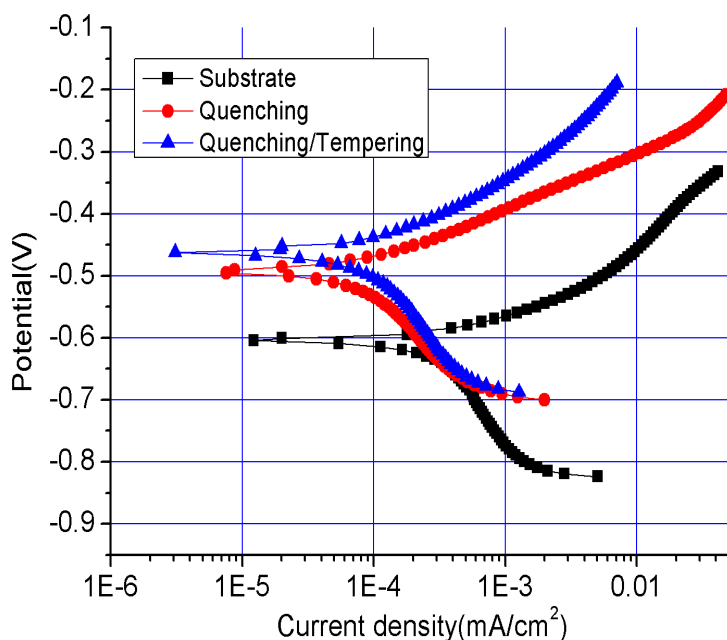


**Figure 6.** Polarization curves for the SPCC steel with and without the induction heat treatments

The anodic Tafel slopes for the SPCC steel specimens with and without the quenching treatment were 0.168 and 0.096 (V/dec), respectively. The deviation of Tafel slope from unity was consistent with electrochemical mechanism that the electron acceptor and donor reactions at the solution/metal interface changed with heat treatments. The corrosion current densities for the SPCC steel specimens with and without the quenching treatment were  $6.66 \times 10^{-5}$  and  $3.78 \times 10^{-4}$  A/cm<sup>2</sup>,

respectively, showing that the corrosion potential and corrosion current shifted, as shown in Fig 6. The corrosion current of the SPCC steel subjected to the quenching treatment is as much as one order of magnitude less than that of the substrate. The SPCC steel subjected to the quenching treatment enhanced the corrosion resistance on the surface, as described above. This result indicates that the corrosion resistance of the SPCC steel varies with the quenching, as well as the quenching/tempering treatments [12]. Meanwhile, grain size discrepancies are caused by the heat treatment process. The corrosion current in specimens were determined to examine the material exposed to quenching/tempering, the quenching treatment and the unmodified substrate. In summary, the induction heat treatment decreases these plane defects and the residual stress that exist in the SPCC steel after the cold rolling process [16-19]. This effect is predominantly attributable to the grain refinement in the case of the heat treatment that enhances the corrosion resistance of the SPCC steel [20].

### 3.3 Mechanical properties

**Table 4.** Mechanical properties of the SPCC steel subjected to various treatments.

	Yield Strength (MPa)	Ultimate tensile strength (MPa)
Substrate	260	370
Quenching	340	413
Quenching/Tempering	300	375

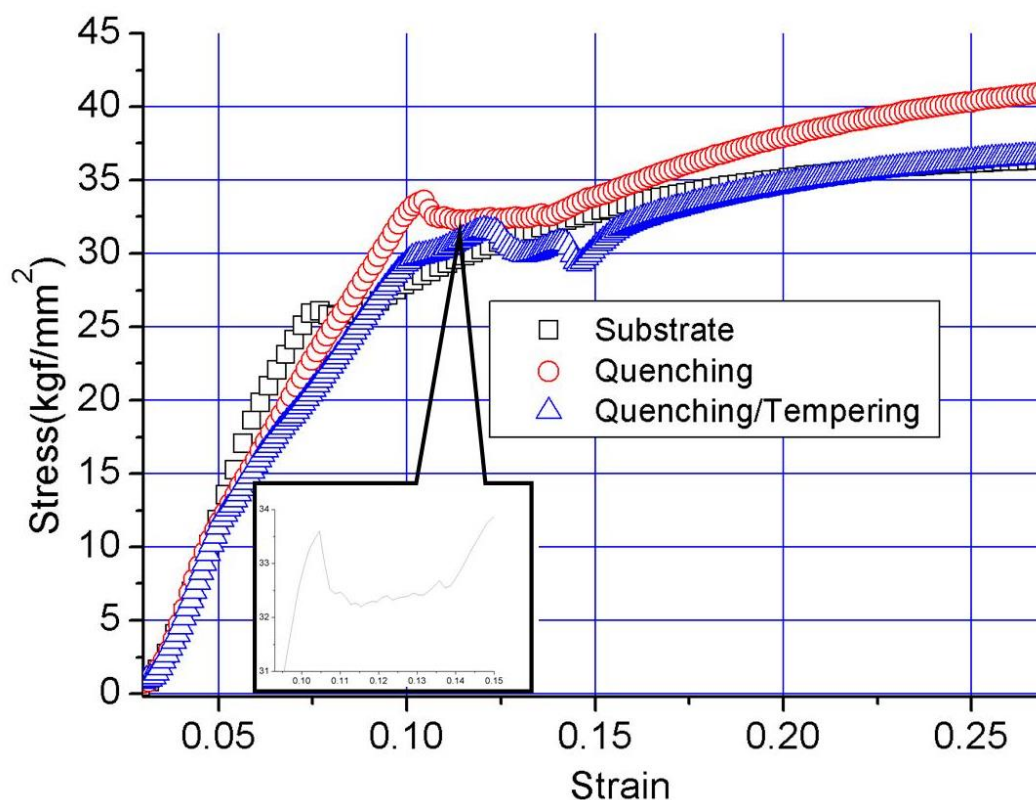


**Figure 7.** Effects of the heat treatment on the tensile properties of the SPCC steel.

The specimen was loaded at a fixed strain rate until fracture. The elastic and plastic regions are shown in the stress-strain diagram in Fig 7. Prior to the loading reaching the critical level (yield stress), the specimen is in the elastic region. Minor plastic behaviour is exhibited after loading to the upper yield point. The appearance of the balance point (lower yield point) is observed as tension continues to be applied and exhibited minor fluctuations, as shown in Fig 7. The upper yield points (as in Table 4) for the substrate and specimen subjected to the quenching treatment were 260 MPa and 340 MPa, respectively. Each fluctuation represents the formation of a Lüders band at the both ends on the specimen [21].

The Lüders band propagates to fill the entire specimen until the end of yielding [22]. It is evident that the toughness of the SPCC steel is improved by the quenching treatment. Furthermore, the obvious yield elongation phenomenon after the quenching/tempering treatment is also observed in the stress strain diagram shown in the inset of Fig 7. Meanwhile, an obvious elongation was found to be associated with the yielding due to the amount of energy available for the precipitation of the carbon atoms after the quench/tempering treatment. As discussed, the geometry of grain causes changes in the SPCC steel, as determined from the macroscopic investigation. The surface tension energy at grain boundaries is strongly correlated to the dislocation mobility [23]. When the specimen is work hardened, the interstitial impurities (carbon atoms) clearly decrease the dislocation mobility energy. The strength and hardness of SPCC steel increases with the grain refinement, shown by the shift in the strain curve from the heat treatment. The experimental results exhibit consistent agreement with the Hall-Petch theory in this study.

#### 4. CONCLUSIONS

Induction heat treatment increases the surface hardness of steel by the magnetic induction effect. In this study, the treatment was employed to modify the properties of SPCC steel using a frequency of 80 kHz at a power of 15 kVA for 2 mins. We demonstrated that the grain geometry is strongly correlated to the corrosion resistance of SPCC steel when exposed to a 5 wt% NaCl environment after heat treatment. The corrosion current in the SPCC steel subjected to the quenching treatment may be as much as one order of magnitude less than seen in the substrate. Finally, the mechanical properties, such as the surface hardness, yield point and tensile strength are also improved by the induction heat treatment. The Hall-Petch relationship was determined to hold true for the present experiment. Additionally, the ductility and corrosion resistance were also modified by the subsequent tempering treatment, with grain growth occurring on the steel surface. The proposed heat treatment improves the overall performance of SPCC steel and promotes its implementation as a potential vehicle material in the near future.

#### References

1. H. Huh, J.H. Yoon, C.G. Park, J.S. Kang, M.Y. Huh and H.G. Kang, *Int. J. Mech. Sci.*, 52 (2010) 745.
2. Y.F. Zhou, W.J. Qiu, W.X. Li and J. Xie, *Adv. Mat. Res.*, 634 (2013) 1698.
3. W.P. Jia, D.Y. Ju and A. Shimamoto, *Key. Eng. Mater.*, 324 (2006) 1229.
4. F. Song, X. Zhang, S. Liu, Q. Tan and D. Li, *Corr. Sci.*, 78 (2014) 276.
5. C. Ma, F. Wu, Y. Ning, F. Xia and Y. Liu, *Ceram. Int.*, 40 (2014) 9279.
6. D. Paquet, J. Lantaigne, M. Bernard and C. Baillargeon, *Int. J. Fatigue.*, 59 (2014) 90.
7. K. Kid, K. Okamoto, M. Ishida, K. Mizobe and T. Shibukawa, *Appl. Mech. Mater.*, 597 (2014) 140.
8. M. D. Eastwood and K. R. Haapala, *Int. J. Adv. Manuf. Tech.*, 80 (2015) 1113.
9. A. H. Seikh, *J. Chem.*, 2013 (2013) 1.
10. A. Ayday and M. Durman, *Mater. Technol.*, 48 (2014) 787.
11. C. Revilla, B. López and J.M. Rodriguez-Ibabe, *Mater. Design.*, 62 (2014) 296.
12. B. H. He, J. J. Sun and Q. A. Tu, *Int. J. Electrochem. Sci.*, 10 (2015) 10631.
13. A.H. Seikh, B. Muneer and H.R. Ammar, *Int. J. Electrochem. Sci.*, 10 (2015) 3054.
14. S. Gao, A. Shibata, M. Chen, N. Park and N. Tsuji, *Mater. Trans.*, 55 (2014) 69.
15. A. H. Cottrell and B. A. Bilby, *Proc. R. Soc. London.*, 62 (1949) 49.
16. T. Balusamy, T. S. N. Sankara Narayanan, K. Ravichandran, I. S. Park and M. H. Lee, *Corr. Sci.*, 74 (2013) 332.
17. Y. Jiao, W. Zheng, D.A. Guzonas, W.G. Cook and J.R. Kish, *J. Nucl. Mater.*, 464 (2015) 356.
18. S.D. Zhang, J. Wu, W.B. Qi and J.Q. Wang, *Corr. Sci.*, 110 (2016) 57.
19. M. A. Amin, M. Saracoglu, N. El-Bagoury, T. Sharshar, Mohamed M. Ibrahim, J. Wysocka, S. Krakowiak and J. Ryl, *Int. J. Electrochem. Sci.*, 11 (2016) 10029.
20. A. A. Aghuy, M. Zakeri, M.H. Moayed and M. Mazinani, *Corr. Sci.*, 94 (2015) 368.
21. T. Vreeland, D.S. Wood and D.S. Clark, *ASM. Inter.*, 33 (1952) 1
22. J. Han, C. Lu, B. Wu, J. Li, H. Li, Y. Lu and Q. Gao, *Mater. Sci. Eng. A.*, 683 (2017) 123.
23. G. Sun, R. Zhou, J. Lu and J. Mazumder, *Acta. Mater.*, 84 (2015) 172.

© 2017 The Authors. Published by ESG ([www.electrochemsci.org](http://www.electrochemsci.org)). This article is an open access article distributed under the terms and conditions of the Creative Commons Attribution license (<http://creativecommons.org/licenses/by/4.0/>).